Top Catal (2013) 56:1088–1095
DOI 10.1007/s11244-013-0074-6

ORIGINAL PAPER

Far Field Combined AFM and Micro-Raman Imaging for Characterisation of Surface of Structured Catalysts: Example of Pd Doped CoO_x Catalysts on Precalcined Kanthal Steel

J. Łojewska · A. Knapik · A. Kołodziej · P. Jodłowski

Published online: 11 July 2013

Abstract A coupled AFM–Raman system was used to study the surface heterogeneity of catalytic materials at various stages of their preparation. The catalysts chosen for the analyses were cobalt oxide with and without palladium dopant deposited on surface of pre-calcined steel carriers. Steel carriers are surveyed here in terms of their application as fillers for structured reactors for the catalytic combustion of volatile organic compounds. Upon steel precalcination stage the interfaced AFM–Raman and in situ Raman analyses revealed the evolution of alumina and iron oxide phases on the surface with their final stable forms found as being α-Al_2O_3 and α-Fe_2O_3. Upon catalyst layering stage AFM–Raman mapping evidenced uniform coverage of precalcined steel carrier with cobalt spinel oxide Co_3O_4. For the doped catalyst except Co_3O_4 palladium(II) oxide grains were also found on the surface. The differences in the composition of cobalt catalysts were correlated with the differences in their catalytic activity.

Keywords AFM–Raman coupled system · AFM–Raman mapping · Cobalt oxide · Catalytic combustion of VOC · Structured reactors

J. Łojewska (✉) · A. Knapik · P. Jodłowski
Faculty of Chemistry, Jagiellonian University, Kraków, Poland
e-mail: lojewska@chemia.uj.edu.pl

A. Kołodziej
Faculty of Civil Engineering, Technical University of Opole, Opole, Poland

1 Introduction

AFM coupled with Raman microscopy is an emerging technique that offers simultaneous analysis of both morphology and texture with the chemical information obtained with high spatial resolution. The system can be harnessed for catalyst design and investigation in a number of ways including combined mapping, with (near field) [1] or without (far field) [2] tip enhanced Raman effect (TERS) as presented in Fig. 1. The principles of AFM–Raman and its applications in catalytic systems can be found in recent review papers [3–8].

In far field mapping the key problem is the differences in spatial resolution of the individual Raman and AFM components of instrumentation. This is particularly evident in coupled maps. The spatial resolution of Raman is governed by the optical diffraction limit in standard confocal microscope systems and is dependent on laser wavelength, objective and confocal coupling. Thus for visible laser μ-Raman spatial resolution does not exceed 200 nm, while AFM can go down to atomic scale.

The interaction of laser light with an AFM tip can improve Raman resolution by a vast array of near field effects [9] among which is enhancement of electric field that occurs on hot spots on surface of tips usually prepared from Au or Ag [1, 2, 5–7]. There plasmon resonance at the surface of a tip (or sample) can occur, thereby increasing a cross section for Raman transitions, and in this way, generating a measured increase in signal intensity. In theory, the Raman enhancement can reach up to 10^6 times but in practice only 10^3 increase has been reported up to now [10].

There are several optical arrangements in which the interfaced AFM–Raman analyses can be performed. Many of them are based on the inverted microscope to analyze transparent samples, usually biological [5]. For non-transparent

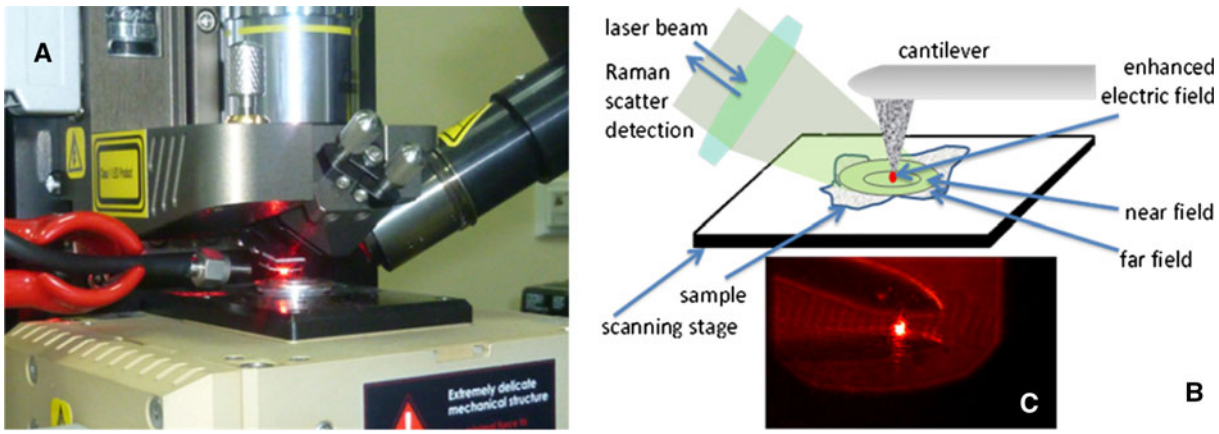

Fig. 1 AFM–Raman configuration **a** a photograph of the AFM with an objective used for Raman analyses, **b** schematics of the AFM–Raman interfaced system, **c** optical microscopic image of a cantilever and laser spot (632 nm laser) taken through AFM optical objective

samples, several different solutions with an aligned [11] and angled optical configuration [10] have been developed to obtain coupled AFM–Raman maps in reflection mode of solid materials, the advantages and disadvantages of which are discussed in [8] (see Fig. 1). The general observation of coupled AFM–Raman system users is that the maps with molecular resolution utilizing the TERS effect are difficult to obtain and can be recorded using the aligned configuration [10].

In this article the AFM–Raman system is used in a far field mode in order to characterize multi-component catalytic materials composed of cobalt, palladium and aluminium oxides. The aim is to demonstrate the applicability of this technique to follow the preparation of catalytic materials and to understand their heterogeneity. The study deals with the preparation of cobalt oxide catalysts doped with palladium on a steel carrier which can be used as a filler for structured converters for VOC combustion as described in our previous papers [12–14]. Here they are used to illustrate the opportunities of the AFM–Raman system.

2 Experimental

2.1 Materials and Catalytic Tests

The samples used for the studies were cobalt oxide catalyst deposited on pre-calcined Kanthal steel sheets (CrAl). Prior to catalyst deposition, the Kanthal sheets were heated in air at 1,000 °C for 24 h to obtain an alumina passive layer (Al_2O_3/CrAl samples). The cobalt oxide catalyst (Co_3O_4/Al_2O_3/CrAl sample) was obtained by impregnation of precalcined steel sheets in water solutions containing cobalt(II) nitrate(V) 0.5 M. To obtain cobalt oxide catalyst doped with palladium (PdO-Co_3O_4/Al_2O_3/CrAl sample), wet impregnation was performed subsequently in 0.1 M tetraamine palladium(II) nitrate(V) solution. After each impregnation step the samples were dried at 100 °C for 10 min and then calcined for 6 h at 600 °C.

TPSR type catalytic tests were performed in a fixed-bed quartz reactor placed in a Catlab instrument (Hiden). The reactor was loaded with a catalyst sample (1 cm × 0.3 cm) and conditioned in 5 % O_2 in He at 500 °C. All experiments were carried out under atmospheric pressure, at a total flow rate of 25 cm^3 min^{-1} over a temperature range of 40–500 °C. The mixture of gases flowing through a reactor contained: *n*-nonane vapour (3,000 ppm) supplied by a saturator fed with He (5 cm^3 min^{-1}), and air (20 cm^3 min^{-1}). The composition of the effluent gas (N_2, CO. CO_2, O_2, H_2O), was analyzed with a quadropole mass spectrometer (QMS). To be able to measure the CO content the apparatus was calibrated for N_2 and H_2O included in air.

2.2 AFM–Raman System

Single Raman spectra were taken using HORRIBA Jobin–Yvon Labram1000 microscope with a 514 nm laser line using a 100× objective and a 600 mm^{-1} grating. Acquisition time for a single spectrum was 30 s.

For in situ measurements the samples were placed in a Linkam temperature cell where they were treated at 1000 °C in air with a flow rate of 20 cm^3 min^{-1}.

The interfaced AFM–Raman experiments were performed using AFM (Park Instruments EX100) with a silicon tip in non-contact mode and a Raman microscope with a long working distance 50× objective at a 60° angle relative to the sample surface (Fig. 1). The laser light was directed to the AFM sample stage and the scattered light directed back to a spectrometer through a coupling optical device. A procedure to align the AFM and Raman maps was devised, and it is presented schematically in Fig. 2a–d. Firstly, AFM topography of the each sample was mapped (a, c). Without changing

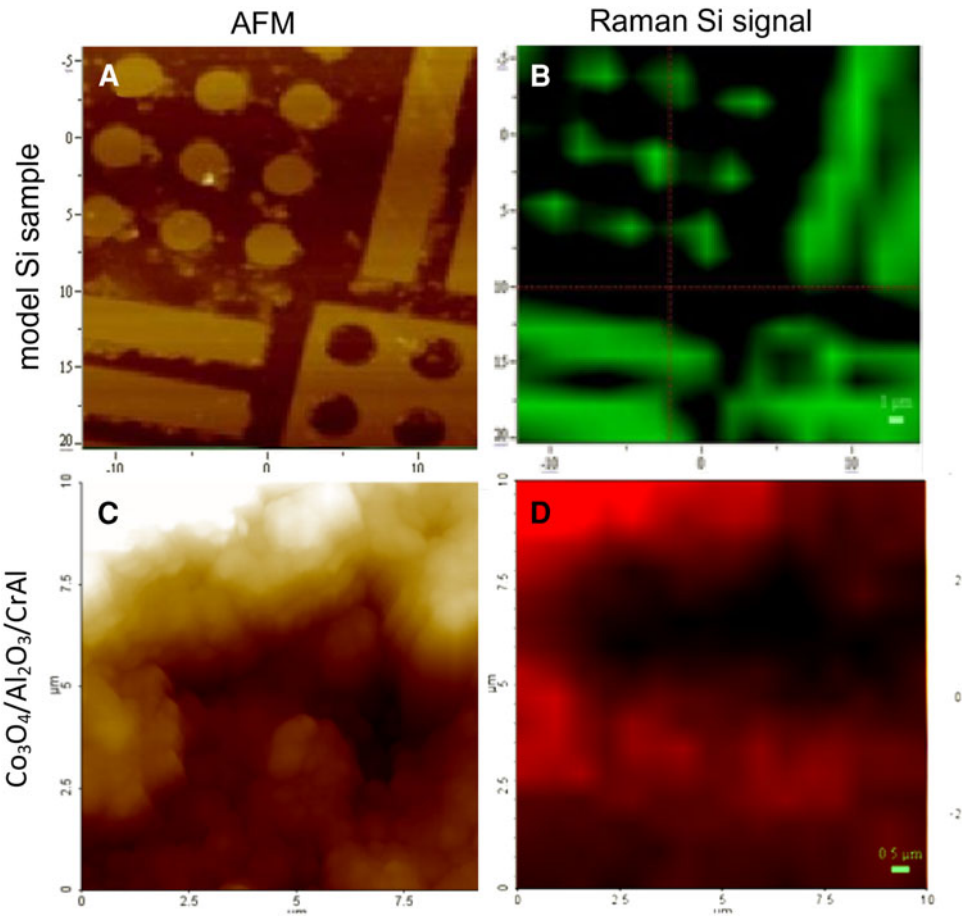

Fig. 2 AFM (***b***, ***d***) and Raman (***a***, ***c***) topography of model Si samples (***a***, ***b***) cobalt catalysts samples (***c***, ***d***)

the position of the sample on the AFM stage a Raman map (of the same dimensions as that used in AFM mapping) was collected using the signal of Si from the AFM tip while scanning the sample (b, d). Then the region of the sample was Raman mapped using the marker bands for a given sample as determined by single spectra measurements collected with the Raman microscope as described above. Each spectrum constituting the Raman map was collected using a 1,800 mm^{-1} grating; acquisition time, depending on the sample, was 1 or 5 s per spectrum measured at each point of a map.

3 Results and Discussion

3.1 AFM and Raman Topography

Coupling AFM and Raman images of a sample surface requires proper alignment of the laser beam on the apex of an AFM tip. This presents a difficult manual task in the angled AFM–Raman configuration used in this study (see Fig. 1). However, the advantage in this case is that the laser beam is large in comparison with AFM tip apex. With this large spot size it is possible to cover both the tip and the sample at the same time as well as to collect Raman signal from both of them. This circumstance was used to obtain the Raman topography maps. During AFM scanning, when the sample moves with the stage under the cantilever (see Fig. 1b), the position of the tip in the z-axis changes with sample topography. On the other hand, the laser position is fixed and the sample movement in the xy plane does not result in z-axis displacement of the laser focal point. As noted above, the AFM tip is displaced in the z-axis relative to the focal point of the laser, and since this tip is prepared from Si, which is a good laser scatterer, the changes of the Raman Si signal intensity can be measured and correlated to the measured AFM-tip displacement. Thereby we can replicate the sample topography on a Raman Si map as shown in Fig. 2c, f. The conformity (or similarity) of the two maps: AFM and Raman Si is a proof for a proper alignment of laser beam on the AFM tip as shown in Fig. 2 by comparison of an image a with b and c with d.

3.2 Coupled AFM–Raman Mapping

3.2.1 Precalcined Kanthal Steel

Kanthal steel is used in our studies as a catalyst carrier. In order to improve the adhesion of the washcoat and catalyst

layer to the surface of the carrier it is pre-treated by high temperature calcination. It is known from our previous studies that pre-calcination of steel sheets at 1,000 °C gives rise to segregation of the alumina layer, 1 μm thick, on top of the steel surface [13]. This layer constitutes a matrix on which cobalt cations attach upon further deposition. The purpose of this part of our research is to show the applicability of the AFM–Raman system to study structure and heterogeneity of the steel surface upon pre-calcination and to finally optimize calcination conditions to generate a stable alumina layer.

From metallurgy it is known that iron, chromium and alumina alloys are rather resistant to oxidation [15]. The α-Al_2O_3 protective layer that is formed upon prolonged oxidation above 1,000 °C protects the steel from further oxidation. XRD [15] and Raman [16] studies of calcined steel alloys show that various alumina phases can be formed at different temperatures. The evolution of oxides formed during calcination of pure Kanthal steel in a flow of air in a temperature cell held at 1,000 °C was followed by in situ Raman analyses (Fig. 3). To avoid casualty the Raman spectra were taken at 4 randomly chosen points on the steel surface (Fig 3a). The Raman spectra were collected at various times during the calcination process as presented in Fig. 3b. After the first minute of oxidation, the α-Fe_2O_3 phase is formed giving rise to appearance of 4 Raman bands at 230, 300, 672 and 1,347 cm^{-1}, which are only a part of a rich vibration pattern of hematite D^6_{3d} group of 7 characteristic frequencies at: 225 and 498 (A_{1g}) and 247, 293, 299, 412 and 613 cm^{-1} (E_g) [17]. A broad band emerging between 1,200 and 1,400 cm^{-1} has been assigned to interactions between two magnons formed on antiparallel spins and is typical of α-Fe_2O_3. After 60 min oxidation the α-Fe_2O_3 pattern disappears from the Raman spectrum as the surface is being covered with transitional δ-Al_2O_3 phase with a characteristic band at 253 cm^{-1} [16]. The first signs of α-Al_2O_3 phase appear after 3 h oxidation in the form of frequencies at 381 and 424 cm^{-1}. At the same analysis time, after having been covered with δ-Al_2O_3 (253 cm^{-1}), islands of α-Fe_2O_3 re-emerge with a characteristic signal at 1,347 cm^{-1}; these islands persist through further oxidation treatment. After 6 h, Raman scattering signals indicate that the δ-Al_2O_3 phase is fully transformed to α-Al_2O_3. Further oxidation did not generate any changes to the Raman spectra. From this the pre-treatment conditioning procedure can be shortened to 6 h instead of the 24 h commonly used.

The γ-Al_2O_3 cubic phase which may also appear on the surface upon calcination at 1,000 °C is not detectable by Raman spectroscopy [18]. According to the XRD studies, γ-Al_2O_3 can be formed at temperatures below 850 °C, δ-Al_2O_3, θ-Al_2O_3 between 850 and 1,000 °C, and above 1,000 °C α-Al_2O_3 [15, 16]. However, XRD and Raman

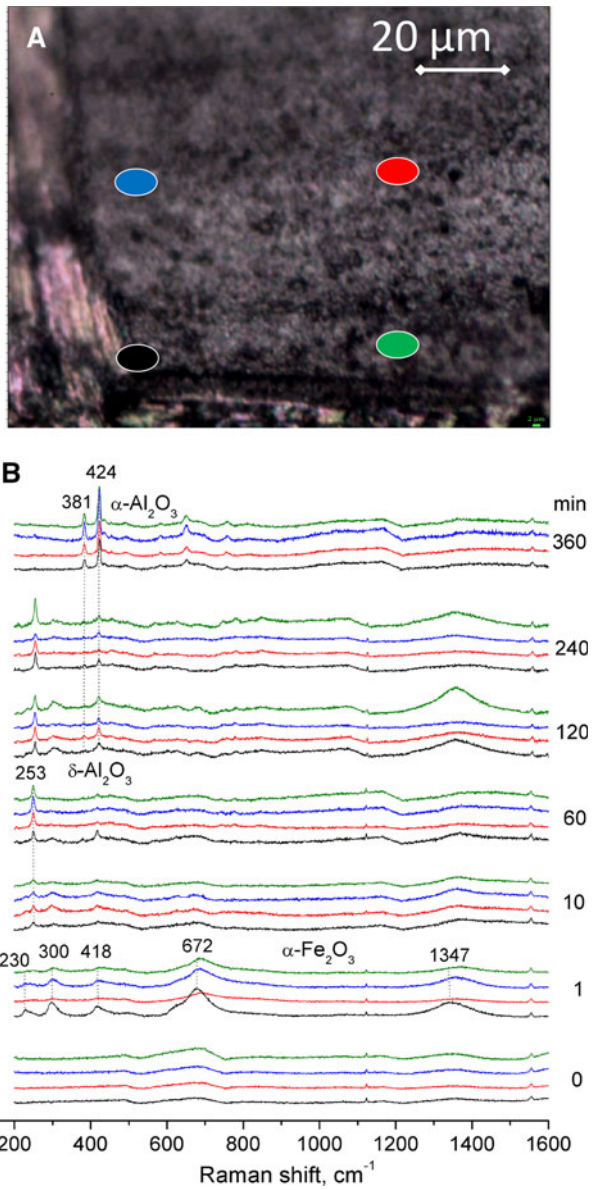

Fig. 3 In situ Raman analyses of Kanthal steel during its precalcination in air at 1,000 °C performed in a temperature cell **a** optical image of the surface with four spots at which Raman spectra were collected, **b** Raman spectra of four spots of Kanthal surface at various times of calcination

studies of Al_2O_3 nanoparticles evidence the coexistence of γ-Al_2O_3 and α-Al_2O_3 phases in the temperature range 1,000–1,050 °C above which the most stable α phase forms.

The heterogeneity of the surface of the pre-calcined steel can be visualised by AFM–Raman mapping in Fig. 4a–d. Judging by the surface topography (AFM image in Fig. 4a, b) there are places which differ in texture, grain size and distribution. One of such spots is presented in Fig. 4a. The magnification of a fragment of the photograph (Fig. 4b) clearly shows the presence of two kinds of grains of different characteristics (compare left-upper and right-

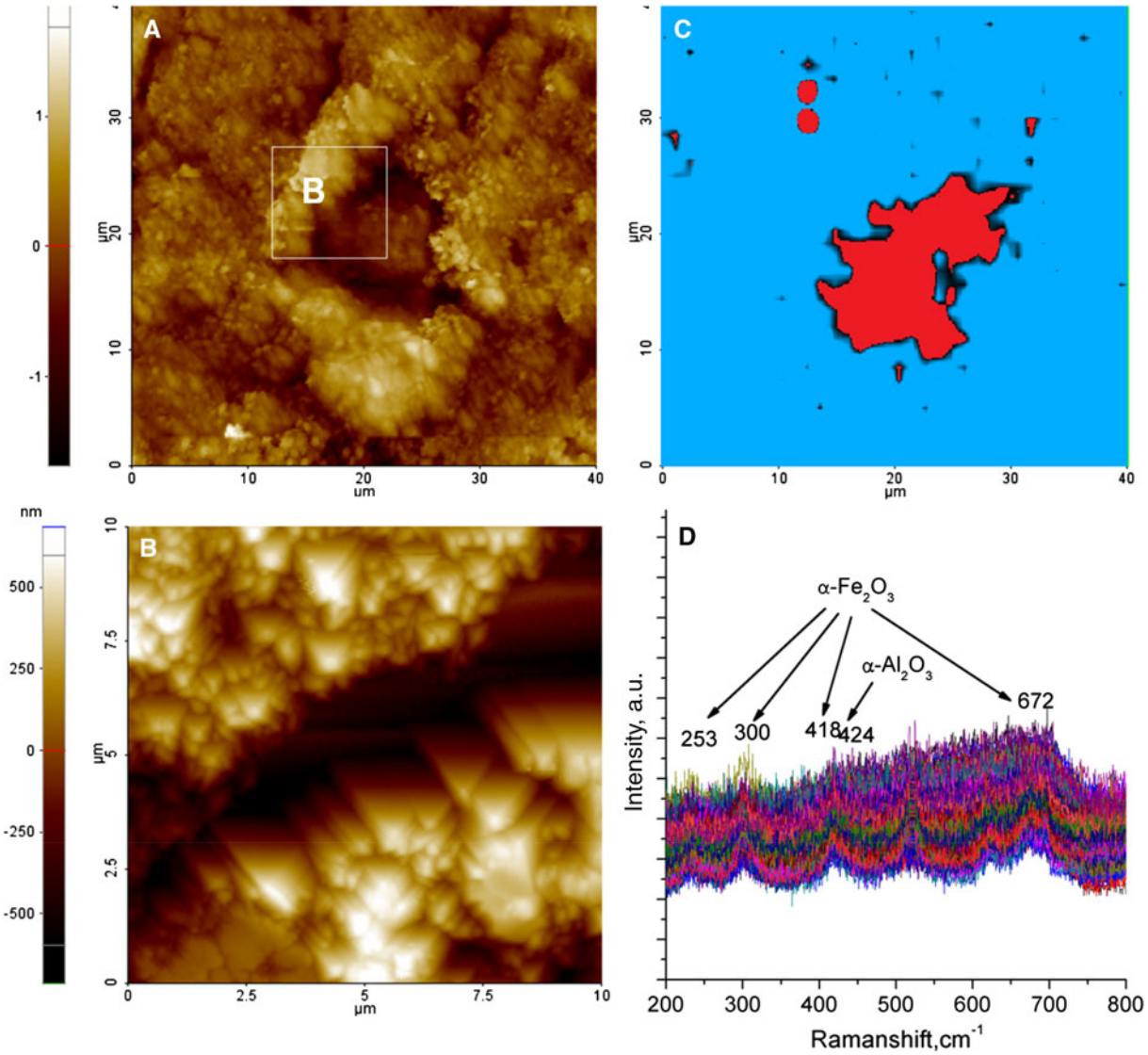

Fig. 4 AFM–Raman analyses of surfaces of pre-calcined Kanthal steel **a** AFM topography map 30 µm × 30 µm, **b** 10 µm × 10 µm fragment of AFM map (a), **c** Raman map 30 µm × 30 µm of the same area (as in a), **d** a stack of Raman spectra collected at each point of the coupled Raman map (map c) obtained using 2 marker bands of α-Al_2O_3 (424 cm^{-1}) and α-Fe_2O_3 (672 cm^{-1})

lower part of the photograph). The Raman map of the same surface area as presented in Fig. 4a, is presented in Fig. 4c. The bench of spectra out of which it was prepared are shown in Fig. 4d. They reveal the presence of α-Fe_2O_3 in the middle of the analyzed area on map 4 C and α-Al_2O_3 in the surrounding area.

3.2.2 Cobalt Oxide Catalyst Surface

The surface of the catalyst samples which were prepared by depositing cobalt oxide (Fig 5) followed by doping with palladium (Fig. 6) were analyzed by interfaced AFM–Raman microscopy. On the surface of the cobalt oxide catalyst cobalt spinel structure was found (Fig. 5c inset). This is confirmed by the presence of 4 vibrations at 468, 515, 614 and 686 cm^{-1} in single Raman spectra, which according to Raman study on Co_3O_4 monocrystal by Hadiyev et al. [19] can be assigned to the E_g, F_{2g}, F_{2g} and A_{1g} symmetry, respectively. In comparison with the single crystal bands they are shifted by a few cm^{-1} (482, 522, 618, 691 cm^{-1}) and are similar to those found by our group for plasma deposited cobalt oxide [20]. In the spectra collected through the AFM–Raman coupling system not all of the bands are easily discernible (Fig. 5c). An intense band at 520 cm^{-1} corresponds to Si from the AFM tip which was not raised during this measurement. The lower accuracy of analyses is due to the fact that the angled objective (Fig. 1), relative to the single spectra measurements collected under the Raman microscope (inset), is less efficient in collecting the signal from Raman scattering.

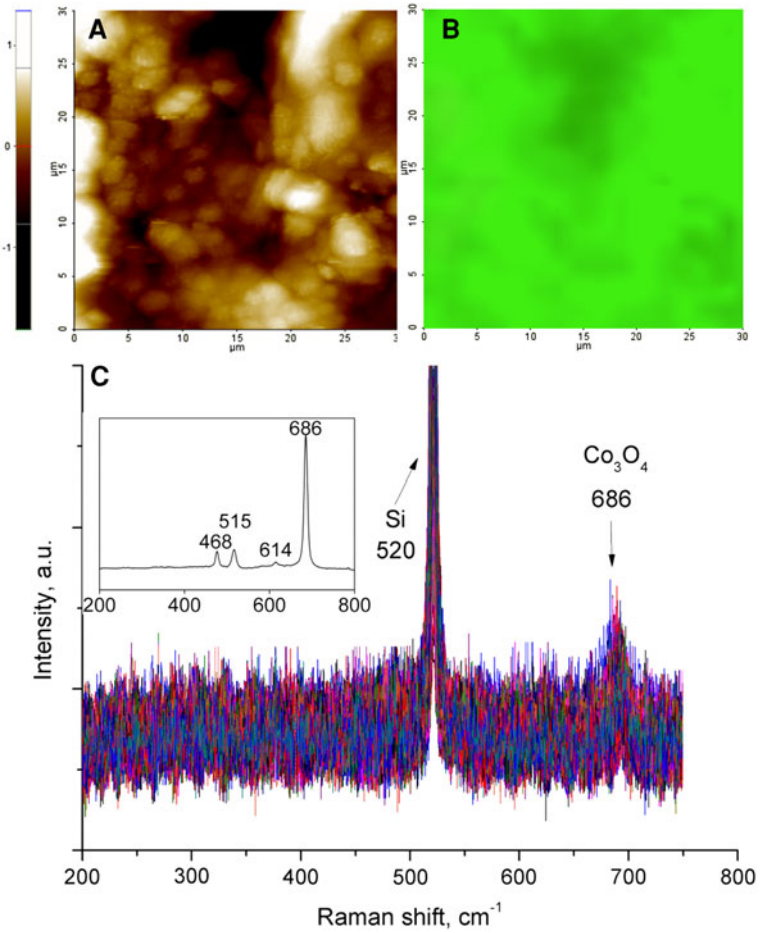

Fig. 5 AFM–Raman analyses of cobalt oxide catalysts deposited on pre-calcined Kanthal steel **a** AFM topography map 30 μm ×30 μm, **b** Raman coupled map 30 μm × 30 μm of the same area as in a obtained using a marker band of Co_3O_4 (686 cm^{-1}), **c** a stack of Raman spectra collected at each point of the coupled Raman map b, Inset–single Raman spectrum of the cobalt catalyst surface collected by confocal Raman microscope

There are also further losses in signal on the mirrors of the coupling system. Therefore, the most intense band at 686 cm^{-1} was chosen as a marker band to prepare the Raman map presented in Fig. 2b. What can be inferred from the Raman map is that the sample of the catalyst is entirely covered with cobalt spinel and no traces of α-alumina and iron oxide phases can be noted in the Raman spectra (Fig. 5c). The differences in the intensity of the spinel signal can be recognized as darker green spots on the Raman map. The intensity pattern on the Raman map relates to the AFM topography shown in Fig. 4a: clearly visible features of the surface such as cavities result in a lower intensity of Raman signal.

The results of analogous analyses for a bi-oxide catalyst composed of cobalt oxide spinel doped with palladium oxide are shown in Fig. 6a–c. The topography of the sample surface fragment (30 μm × 30 μm) is presented in Fig. 6a. There, a large grain of around 5 μm in diameter protruding from the surface can be noted. The presence of palladium(II) oxide is evidenced by the intense band at 654 cm^{-1} [21] in the Raman spectra collected by the interfaced system. The cobalt spinel pattern is again easily distinguished in the collected spectra (Fig. 6c), however, the band positions are slightly shifted in comparison with the pure cobalt oxide sample. The Raman map (Fig. 6b) was built using 2 marker bands one for cobalt spinel (694 cm^{-1}) and the second for palladium oxide (654 cm^{-1}). It is then possible to assign the grain found in the middle of the AFM image to palladium oxide. It should be noted here that the resolution of Raman map is lower than that of AFM as the size of the palladium spot found on the Raman map is larger than a grain found on the AFM map. This fact has been pointed out in the introduction. The problem of the compatibility of AFM and Raman resolutions is also due to the fact that two adjacent points measured on the Raman map bear the information partly of the same surface area covered by a laser spot directed to the sample surface upon scanning it on the AFM stage. Traces of palladium(II) oxide can also be noted on the Raman map at the other places of the Raman map (lower right corner of the map 6 B) although at a first glance there are no differences in grains shapes on the AFM image at this spot.

The modifications in composition of the samples comply with the changes in their activity studied by TPSR in oxidation of *n*-nonane and presented in Fig. 7. In general, the activity of both samples is much higher than that of the

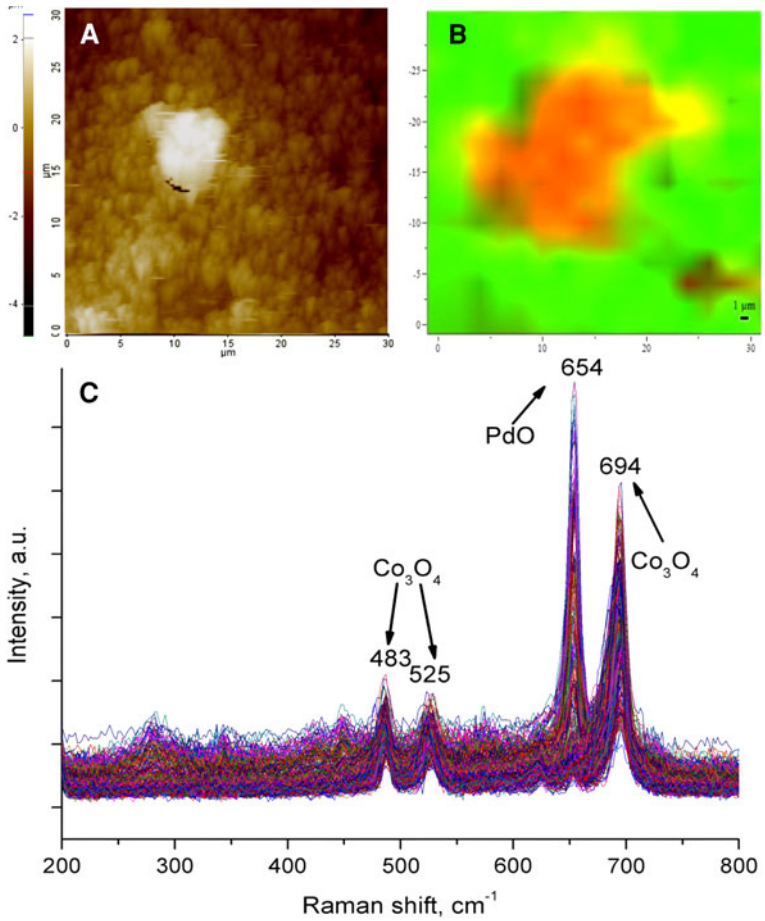

Fig. 6 AFM–Raman analyses of cobalt oxide catalysts doped with palladium deposited on pre-calcined Kanthal steel **a** AFM topography map 30 μm × 30 μm, **b** Raman coupled map 30 μm × 30 μm of the same area (as in a) obtained using two marker bands of Co_3O_4 (686 cm^{-1}) and PdO (654 cm^{-1}), **c** a stack of Raman spectra collected at each point of the coupled Raman map b

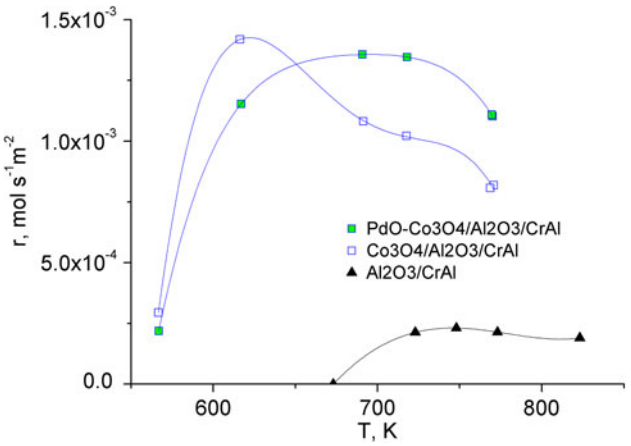

Fig. 7 Catalytic TPSR tests of the three studied samples in catalytic combustion of *n*-nonane

initial undeposited precalcined Kanthal steel. The differences between two catalysts occur at the lower temperature range (<650 K) in which the palladium doped catalyst is more active than a pure cobalt spinel catalyst which agrees with the general knowledge. The palladium doped sample, is however less temperature resistant and loses its activity above 650 K where cobalt spinel remains active. This behaviour may be connected with the palladium grains sintering. Conversely, activity loss of the cobalt catalyst above 750 K is a result of typical reaction rate limitation caused by diffusional resistance [22].

4 Conclusions

The case study of a coupled AFM–Raman survey of cobalt oxide palladium doped catalysts deposited on metallic carriers is one of the first attempts of characterization of catalytic materials using the far field operational mode of this instrumentation. The coupled AFM–Raman mapping combined with in situ investigation of catalysts surface at various stages of its preparation can help grasp the catalyst material heterogeneity.

Upon pre-calcination of Kanthal steel, which is used in our study as a catalyst carrier and a filler of structured reactors, various phases of alumina segregating on the surface were distinguished upon its in situ calcination at 1,000 °C. However, the stable final composition of the surface was found to be α-Al_2O_3 and α-Fe_2O_3. These phases were distinguished on coupled AFM and Raman maps.

The AFM–Raman mapping also shows that the surface of the cobalt oxide catalyst obtained by impregnation of pre-calcined Kanthal steel is uniformly (with the accuracy of around 1 μm) covered with the grains of cobalt oxide spinel and no alumina and iron oxide phase is present on the surface. AFM–Raman mapping of samples doped with palladium, reveals the presence of palladium(II) oxide formed as grains of various sizes which are located on top of cobalt spinel oxide. The differences in the exemplary samples composition were reflected by the differences in their activity studied in oxidation of *n*-nonane: the doped samples showing higher activity at lower temperature range (<650 K).

Acknowledgments The research was done within BRIDGE Programme Grant (No 2010-1/4) from the Foundation for Polish Science, co-financed by the EU, and a Grant from Nation Science Centre N N523 556638. The authors are grateful to SPB 811/N-COST/2010/0 for sponsoring optical parts to Raman/AFM system.

References

1. van Schrojenstein Lantman EM, Deckert-Gaudig T, Mank AJG, Deckert V, Weckhuysen BM (2012) Nat Nanotechnol 7:583–586
2. Diskus M, Nilsen O, Fjellvåg Hr, Diplas S, Beato P, Harvey C, van Schrojenstein Lantman E, Weckhuysen BM (2012) J Vac Sci Technol A 30:01A107
3. Bailo E, Deckert V (2008) Chem Soc Rev 37:921
4. Pettinger B, Domke KF, Zhang D, Schuster R, Ertl G (2007) Phys Rev B 76:113409
5. Yeo B-S, Stadler J, Schmid T, Zenobi R, Zhang W (2009) Chem Phys Lett 472:1–13
6. Chan KLA, Kazarian SG (2011) Nanotechnology 22:175701–175705
7. Kim H, Kosuda KM, Van Duyne RP, Stair PC (2010) Chem Soc Rev 39:4820–4844
8. Berweger S, Raschke MB (2010) Anal Bioanal Chem 396:115
9. Novotny L, Stranick SJ (2006) Annu Rev Phys Chem 57:303–331
10. Pettinger B, Ren B, Picardi G, Schuster R, Ertl G (2004) Phys Rev Lett 92:096101
11. Harvey CE, van Lantman EMS, Mankab AJG, Weckhuysen BM (2012) Chem Commun 48:1742–1744
12. Łojewska J, Kołodziej A, Łojewski T, Kapica R, Tyczkowski J (2009) Appl Catal A 366:206–211
13. Łojewska J, Kołodziej A, Dynarowicz-Łątka P, Wesełucha-Birczyńska A (2005) Catal Today 101:81–91
14. Kołodziej J Łojewska, Jodłowski P, Tyczkowski J, Redzynia W, Zapotoczny S, Kuśtrowki P (2012) Chem Eng J 200–202: 329–337
15. Steinmetz P, Wright IG, Galerie A, Monceau D, Mathieu S (2008) Mater Sci Forum 7:915–922
16. Deo G, Hardcastle FD, Richards M, Hirt AM, Wachs IE (1990) ACS Symp Ser 437:317–328
17. de Faria DLA, Venaüncio Silva S, de Oliveira MT (1997) J Raman Spectr 28:873–878
18. Cava S, Tebcherani SM, Souza IA, Pianaro SA, Paskocimas CA, Longo E, Varela JA (2007) Mater Chem Phys 103:394–399
19. Hadjiev VG, Iliev MN, Vergilov IV (1988) J Phys C 21:L199
20. Tyczkowski J, Kapica R, Łojewska J (2007) Thin Solid Films 15(16):6590–6595
21. Baylet A, Marécot P, Duprez D, Castellazzi P, Groppi G, Forzatti P (2011) Phys Chem Chem Phys 13:4607–4613
22. Ochońska J, McClymont D, Jodłowski PJ, Knapik A, Gil B, Makowski W, Łasocha W, Kołodziej A, Kolaczkowski ST, Łojewska J (2012) Catal Today 191:6–11